Channel Model for the Surface Ducts: Large-Scale Path-Loss, Delay Spread, and AOA

Ergin Dinc, *Student Member, IEEE*, and Ozgur B. Akan, *Senior Member, IEEE*

***Abstract*—Atmospheric ducts, which are caused by the rapid decrease in the refractive index of the lower atmosphere, can trap the propagating signals. The trapping effects of the atmospheric ducts can be utilized as a communication medium for beyond-line-of-sight (b-LoS) links. Although the wave propagation and the refractivity estimation techniques for the atmospheric ducts are well studied, there is no work that provides a channel model for the atmospheric ducts. Therefore, we develop a large-scale path-loss model for the surface ducts based on the parabolic equation (PE) methods for the first time in the literature. In addition, we develop a ray-optics (RO) method to analyze the delay spread and angle-of-arrival (AOA) of the ducting channel with the surface ducts. Using the developed RO method, we derive an analytical expression for the effective trapping beamwidth of the transmitter to predict the ranges of the beamwidth that can be trapped by the surface ducts according to the refractivity and the channel parameters.**

***Index Terms*—Communication channels, delay estimation, propagation, ray-tracing, refraction, surface duct.**

I. Introduction

ATMOSPHERIC ducts are caused by nonstandard atmospheric conditions, and wave propagation in the presence of atmospheric ducts is called anomalous wave propagation [1]. An atmospheric duct is a layer in which rapid decrease in the refractivity of the lower atmosphere occurs. In this way, atmospheric ducts can trap the propagating signals as shown in Fig. 1. Most of the signal energy propagates in ducting layer unlike standard atmosphere. Therefore, trapped signals can propagate through beyond-line-of-sight (b-LoS) distances with lower path-loss values.

Modern naval b-LoS systems mostly utilize Satellite Communications (SATCOM). However, SATCOM has capacity problems under low coverage and high transmission delays. In addition, the range of direct communication systems depends on the height of transmitter towers. Generally, it is expensive or not possible to use high transmitter towers to monitor coastal areas. Therefore, Woods *et al.* [2] provides the implementation of ducting channel for a 78-km link with low-height antennas to monitor a reef site. According to their results, atmospheric ducts can provide 10 Mbps for 80% of the time at 10.5 GHz. Based on our reviews [3], ducting channel b-LoS communications can connect distances up to 500–1000 km in coastal and maritime environments, because duct formation is more probable in regions with high humidity.

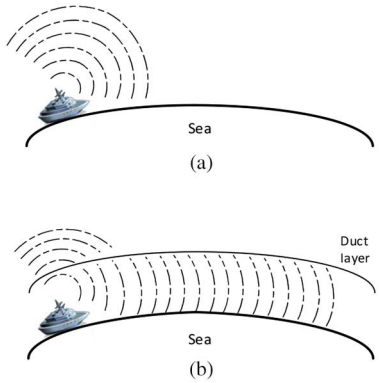

Fig. 1. Signal spreading in (a) standard atmosphere and (b) duct.

Although wave propagation and refractivity modeling of atmospheric ducts are well-studied topics [3], there is no work that considers channel modeling for atmospheric ducts. In addition, available studies cannot estimate large-scale and small-scale characteristics of ducting channels. Since ducting-channel communication can be a promising candidate for b-LoS communications, we aim to develop a large-scale path-loss model for surface ducts and analyze delay spread and AOA of surface ducts for the first time in the literature. In this way, development of large-scale path-loss model enables us to make link budget calculations faster for different channel and duct parameters. In addition, small-scale path-loss, *fading*, characteristics of the channel can be predicted as well.

The contributions of this paper is trifold. First, we develop a statistical large-scale path-loss model for surface ducts based on parabolic equation (PE) simulations. The developed large-scale path-loss model is utilized to predict the distribution of small-scale fading, and communication ranges that can be provided by surface ducts via link budget analysis. We utilize PE methods to estimate the path-loss for atmospheric ducts because ray-tracing and normal modes techniques are both unreliable and too resource-consuming under nonstandard atmospheric conditions [4]. The proposed large-scale path-loss model can estimate path-loss results for changing duct heights and channel parameters. Therefore, the developed method can provide fast estimates of path-loss under varying channel conditions. In addition, we develop a ray-optics (RO) method to calculate ray trajectories with surface ducts. By using the developed method, we analyze delay spreads to determine the fading behavior of the channel. Available studies do not provide a realistic analysis for the delay spread of ducting channels. Lastly, we

Manuscript received November 09, 2014; revised February 15, 2015; accepted March 25, 2015. Date of publication April 02, 2015; date of current version May 29, 2015.

The authors are with the Next-Generation and Wireless Communications Laboratory, Department of Electrical and Electronics Engineering, Koc University, Istanbul 34450, Turkey (e-mail: edinc@ku.edu.tr; akan@ku.edu.tr).

Color versions of one or more of the figures in this paper are available online at http://ieeexplore.ieee.org.

Digital Object Identifier 10.1109/TAP.2015.2418788

develop an analytical formula to determine the effective trapping beamwidth, which represents the range of beamwidths that can be trapped by surface ducts according to the channel conditions. Signals cannot be trapped by surface ducts beyond the effective trapping beamwidth and their power propagates through troposphere. Energy of these signals is wasted in b-LoS systems. For this reason, we develop an analytical formula which can help both academia and system designers while designing efficient b-LoS communication links with atmospheric ducts.

This paper is organized as follows. Section II provides related works. Section III includes refractivity models of atmospheric ducts. In Section IV, we review both PE and RO methods to model surface ducts. In addition, this section includes the derivation of RO methods for surface ducts and the effective trapping beamwidth. Section V provides the derivation of large-scale path-loss model for surface ducts. In Section VI, simulation results are presented for delay spread, AOA, and path-loss of the channel under various cases. Finally, conclusion is presented in Section VII.

II. Related Work

Ducting-channel studies can be divided into two main parts: refractivity estimation and wave propagation studies. Refractivity estimation techniques aim to predict the vertical refractivity gradient which is essential to model the wave propagation at the lower atmosphere. There are various methods for predicting the refractivity of the lower atmosphere: the direct measurement techniques such as microwave refractometers and radiosonde balloons [5], LIDAR (Light Detection and Ranging) techniques [6], *in situ* bulk measurements and meteorological methods [7], GPS (Global Positioning System) measurements [8], and refractivity from clutter techniques [9], [10]. In this study, we utilize the refractivity measurement results presented in [11], which is based on the atmospheric measurements in Istanbul, Turkey, and [12] on the microwave refractometer measurements with a helicopter in Wallops Island, VA. We determine the parameters regarding to characterize the surface ducts as suggested in [11] and [12].

Since RO-based techniques [13] or normal-modes-based techniques [13], [14] are unreliable or too resource-consuming, ducting channel propagation studies mostly focus on PE methods that utilize the paraxial approximation to the wave equation. PE can be solved with numerical methods: split-step Fourier (SSF), finite difference (FD), and finite element (FE). Especially with the development of SSF methods [15], PE has become the most popular method to model anomalous wave propagation [1], [2], [16], [17], because SSF methods provide fast and reliable results. In addition, PE methods can take the refractivity conditions as input and they can effectively model the complex boundary conditions. Good review of ducting channel wave propagation modeling and SSF-based PE method can be found in [3] and [4], respectively.

To model wave propagation in ducting channel, there are available wave propagation tools. The most widely used one is AREPS that is developed by the Atmospheric Propagation Branch at the Space and Naval Warfare Systems Center, San Diego [18]. Combination of RO and PE methods is also promising as suggested in [19]–[22]. Therefore, AREPS utilizes both RO and SSF-based PE methods. In addition, PETOOL [23], which is also based on SSF, is capable of modeling both forward and backward scattered waves under different terrain and refractivity conditions. Therefore, PETOOL is promising especially for regions with irregular terrain conditions. Since PETOOL is a free and online available tool and it is calibrated with RO methods and AREPS as described in [23], we utilize PETOOL to model the surface ducts. In addition, we make RO analysis to the surface ducts to estimate the delay and AOA of the channel. Therefore, characteristics of the channel can be estimated with hybrid methods as suggested in [19] and [20].

There are experimental studies about ducting channel wave propagation. Woods *et al.* [2] provides a high data rate employment of the atmospheric ducts for b-LoS sensor networks. In [2], the authors observed that wave propagation analysis performed in AREPS has strong consistency with the experimental results. In addition, Refs. [24]–[27] compare the simulation results with the PE methods and the experimental measurements for an 83-km link at 4.7, 10, and 15 GHz. According to their results, the region had strong evaporation ducts, and the experimental path-loss measurements were consistent with the PE simulations. Furthermore, Hitney *et al.* [1] provides one of the most extensive review of ducting channel with comparison of PE-based results and experimental results for surface-based ducts. The results of this work show that surface-based ducts can provide 10–20 dB less path-loss compared to free space at b-LoS distances. Similar experimental results to verify PE simulations is presented in [28] as well. To sum up, the results of PE methods are validated through a number of different experimental works for different type of ducts. As a result, theoretical results that are generated with PE-based tools can be considered as reliable based on previous experimental validations.

III. Refractivity

Atmospheric ducts are formed by nonstandard atmospheric conditions. Formation and characteristic of atmospheric ducts depend on refractivity of the lower atmosphere. Therefore, we review refractivity and modified refractivity to characterize atmospheric ducts.

Tropospheric radio refractive index (n) changes slightly with the atmospheric parameters: wind, temperature, pressure and humidity at the lower atmosphere. n varies in the order of 10^{-3}. Therefore, refractivity is utilized instead of refractive index and refractivity (N) is given as [29]

$$N = (n-1) \times 10^6 \,\text{N-units} \tag{1}$$

where n is the atmospheric refractive index.

Trapped signals in ducting layer have low grazing angles. Therefore, refractivity model should consider the curvature of the earth. Thus, modified refractivity (M) is defined as [29]

$$\begin{aligned} M &= N + \left(\frac{h}{R_0}\right) \times 10^6 \\ &= N + 157 \times h \,\text{M-units} \end{aligned} \tag{2}$$

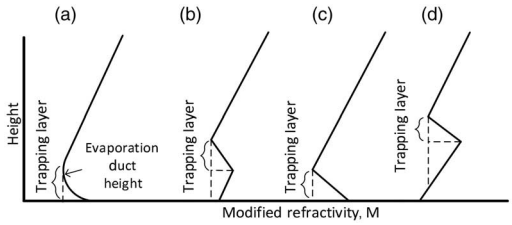

Fig. 2. Modified refractivity profiles of atmospheric ducts. (a) Evaporation duct. (b) Surface-based duct. (c) Surface duct. (d) Elevated duct.

where h is the height above the surface level in km and R_0 is the earth radius in km.

According to the modified refractivity gradient, there are four different refractive conditions. In subrefraction condition ($\partial M/\partial z > 157$ M-units/km), signal rays are refracted away from ground through atmosphere. Standard refractivity condition is associated with (157 M-units/km $\geq \partial M/\partial z >$ 78 M-units/km) and this condition represents standard wave propagation. Signals propagate downward in super-refraction condition (78 M-units/km $\geq \partial M/\partial z > 0$ M-units/km). Most importantly, trapping condition, which is also known as *ducting condition*, is associated with $0 \geq \partial M/\partial z$, and signal rays are trapped between surface and ducting layer. This effect can make trapped signals to propagate over-the-horizon with low path-loss. For the formation of atmospheric ducts, humidity is an essential factor [3]. Thus, ducting channel is a promising candidate for b-LoS communications especially in coastal and maritime environments as reviewed in [3].

There are four types of atmospheric ducts according to their formation process and refractivity profiles: 1) evaporation ducts; 2) surface-based ducts; 3) elevated ducts; and 4) surface ducts. As in Fig. 2(a), the modified refractivity of evaporation ducts can be modeled with a logarithmic function [30]

$$M(z) = M_0 + 0.125z - 0.125\delta \ln\left(\frac{z+z_0}{z_0}\right) \qquad (3)$$

where M_0 is the value of modified refractivity at the surface which is taken as 315 M-units [31], z is the vertical height, δ is the duct height, and z_0 is the aerodynamic roughness length which is assumed as 1.5×10^{-4} m [30].

Surface-based and elevated ducts are modeled with a trilinear curve as in Fig. 2. Surface ducts are modeled with a bi-linear curve as in Fig. 2(c). Since evaporation ducts are modeled with the logarithmic function, evaporation ducts are complex to be analyzed with RO-based tools. As a result, we only consider surface ducts in this paper. However, an evaporation duct and a surface duct having the same duct height is expected to have similar maximum delay spread and AOA, because their refractivity profiles are closer as in Fig. 2. Thus, results presented for surface ducts can be utilized to predict the characteristics of evaporation ducts as well.

In this paper, surface ducts are characterized with two atmospheric parameters: duct height (δ) and duct strength (ΔM). Duct height is the height where the gradient of modified refractivity changes its sign as in Fig. 2(c). Duct strength is the amount of change in modified refractivity from the bottom to the top of the surface duct. Modified refractivity above surface duct is assumed as standard condition and decreases with 118 M-units/km. We utilize the experimental surface duct measurements [11], [12] to determine duct height and duct strength parameters.

IV. Channel Modeling Techniques for Surface Ducts

Ducting channel wave propagation requires modeling of atmospheric parameters and complex boundary problems. Therefore, PE methods are preferred for estimating path-loss in ducting channels. In addition, we utilize RO methods to analyze delay spread and AOA of ducting channel with surface ducts. In this section, we first review PE and develop a RO-based method to analyze delay spread and AOA of ducting channels.

A. Parabolic Equation Methods

Parabolic equation (PE) methods use paraxial approximation to the Helmholtz wave equation, and it was originally developed in [32]. PE methods are capable of modeling the complex boundary conditions and the refractivity variations of the lower atmosphere [33]. Especially with the derivation of a simple solution to PE based on split-step Fourier (SSF) method [15], PE methods became the dominant technique to model the wave propagation in ducting channels. Although there are other numerical methods to solve PE, finite difference (FD) and finite element (FE), SSF method is more preferable with its accuracy and computational efficiency [1], [3], [4], [18], [34].

Formulation of PE for the electromagnetic problems is summarized in [35]. The theory of PE is explained in detail in [1], [33], [36]. Interested reader may refer to these references. However, we do not discuss the theory of PE in this paper. Instead, we review how path-loss calculations are performed with PE methods. For two-dimensional (2-D) narrow angle forward scatter waves, PE in scalar form is given as [4]

$$\frac{\partial u(x,z)}{\partial x} = \frac{i}{2k}\frac{\partial^2 u(x,z)}{\partial z^2} + \frac{ik}{2}(m^2(x,z)-1)u(x,z) \qquad (4)$$

where k is the wave number, $m = 1 + M10^{-6}$ is the modified refractive index, $u(x,z)$ is the reduced function, x represents the horizontal axis, and z represents the vertical axis (height). Equation (4) can be used for both horizontal and vertical polarization.

We utilize PETOOL [23], which is a free on-line available tool based on the PE method with SSF, to solve (4). As discussed in Section II, PETOOL is calibrated with AREPS which is an experimentally validated tool. With PE methods, path-loss (PL) can be found using $u(x,z)$ as [33]

$$PL = 20\log(4\pi/|u(x,z)|) + 10\log(r) - 30\log(\lambda) \qquad (5)$$

where λ is the wavelength and r is the range. Unlike available propagation studies, we utilize PE methods to develop a large-scale path-loss model for the first time in the literature in Section V.

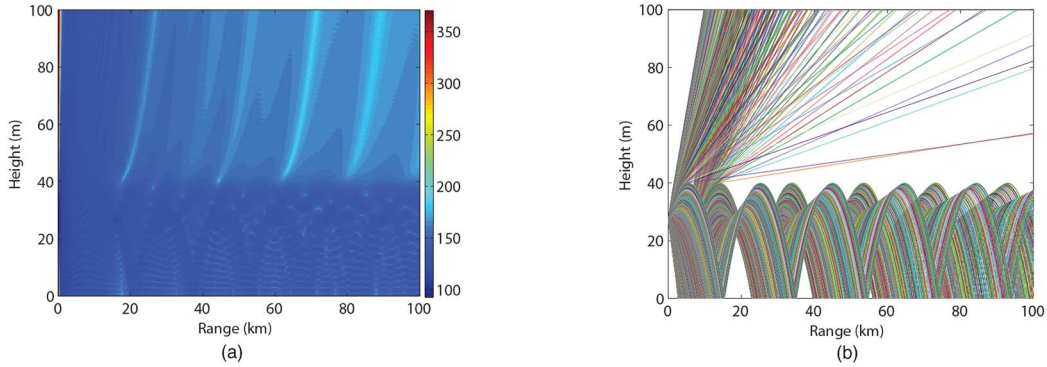

Fig. 3. Wave propagation results with (a) PETOOL and (b) RO methods for 40-m surface duct, 10 GHz, 27-m transmitter height.

B. Ray-Optics Methods

Although PE methods dominate ducting channel wave propagation modeling, RO methods can be utilized to estimate delay spreads and propagation angles [33], [37] as in hybrid models [18], [19]. In addition, [38] provides the comparison of AOA predictions with RO methods and the experimental observations. According to their results, the predicted AOA values were consistent with the observations. Since PE methods are not capable of estimating delay spreads and AOAs, RO methods are promising for the channel modeling in ducting layer.

RO methods utilize the well-known Snell's equation. By solving the Snell's equation for stratified atmosphere, the Eikonal equation is derived to calculate trajectory of each ray. Trajectories of rays are utilized to calculate delay spreads and AOA of the channel. There are some studies in the literature which focus on ray-tracing simulations to model wave propagation in atmospheric ducts. In [39], [40], ray-tracing analysis is performed to estimate delay in elevated ducts, but their models assume that only three rays can reach to the receiver. According to these papers, an 80-km link with elevated ducts shows a few nanosecond delay spread. In [41], [42], they assume that odd number of rays can reach to the receiver and estimate AOA with the ray-tracing simulations for surface-based ducts. Although existing studies have significant results for ducting channel, more realistic results can be generated with RO methods. Therefore, we utilize RO methods to estimate the fading characteristics of the channel and the distribution of AOA for surface ducts. Lastly and more importantly, we derive an analytical expression for the maximum and minimum value of the angle-of-departure (AOD) which can be trapped by surface ducts. With the derived expression, transmitter can be designed to maximize the efficiency of the system by only propagate in the calculated beamwidth span.

The remaining of the section includes derivation of ray trajectory formula and derivation of trapping beamwidth.

1) Ray Trajectories: Ray trajectories in atmospheric ducts can be estimated with RO methods [37]. However, RO methods become more reliable above 3 GHz [29]. Since evaporation ducts perform with lowest path-loss near 10 GHz [2], [3], [16], we aim to focus 5–15 GHz frequency range in this paper. The main drawback of RO methods is the inefficiency to include the effects of frequency. However, the results generated with RO methods show high consistency with PE results as in Fig. 3 as suggested in [38].

In [43], the earth is assumed as flat for the ray-tracing simulations. However, the curvature of the earth becomes important at b-LoS distances. Therefore, we utilize the earth radius transformation and the Snell's law to find the Eikonal equation for surface ducts by assuming the atmosphere has infinitesimal stratified layers. In this way, ray trajectories can be estimated with the Eikonel equation which is represented as

$$\frac{1}{n(z)}\frac{dn}{dz} - \frac{1}{R_0} = \frac{d^2z}{dx^2} \tag{6}$$

where R_0 is the radius of the earth which is used as 6370 km, and the derivation of (6) can be found in Appendix A. $n(z)$ shows very slight variations with the height which is in the order of 10^{-3} [44]. Therefore, (6) is simplified as

$$\frac{1}{n(0)}\frac{dn}{dz} - \frac{1}{R_0} = \frac{d^2z}{dx^2} \tag{7}$$

where $n(0)$ is used as 1.00035 [44].

Since surface ducts have a bilinear refractivity model as in Fig. 2, (6) can be solved as described in Appendix B and ray trajectories are calculated as

$$z = \frac{1}{2}\left(\frac{1}{n(0)}\frac{dn}{dz} - \frac{1}{R_0}\right)x^2 + \theta x + h_t \tag{8}$$

where θ is the angle of the ray with respect to the ground at the transmitter. Equation (8) can be solved step by step for each ray to calculate the trajectory of the trapped paths.

Fig. 3(b) shows the ray trajectories for a 40-m surface duct ($\Delta M = 20$ M-unit), and Fig. 3(a) presents path-loss results for the same ducting conditions by using PETOOL with the following channel parameters: 27-m transmitter, horizontal polarization, and 10 GHz. As noticed, regions with high ray densities are associated with low path-loss values. In addition, shadowed regions are located at the similar locations in both figures. Therefore, PE methods and RO methods give consistent results.

2) Trapping Beamwidth: According to the channel geometry and atmospheric conditions, only rays that have certain angles can be trapped by atmospheric ducts. Rays outside of this certain range cannot be trapped and propagate through the

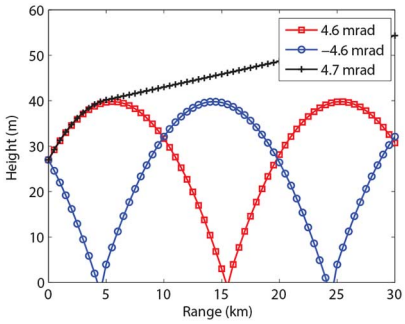

Fig. 4. Ray trajectories with the ray-tracing method.

atmosphere. Energy of these rays are wasted in b-LoS systems. To increase the efficiency, we develop an analytical model to estimate the effective trapping beamwidth at the transmitter side for the first time in the literature.

By utilizing the proposed ray trajectory formula (8), we derive the span of effective trapped beamwidths which depends on the change in the refractive index, transmitter height, and duct height. The derivation of maximum and minimum trapping beamwidths ($\theta^T_{max,min}$) can be found in Appendix C, and $\theta^T_{max,min}$ are found as

$$\theta^T_{max,min} = \pm\sqrt{2\left(\frac{1}{n(0)}\frac{dn}{dz} - \frac{1}{R_0}\right)(h_t - \delta)}. \tag{9}$$

In trapping layer, refractive index decreases with height, and this implies that $\frac{dn}{dz} < 0$. In addition, our model assumes that transmitter is located within surface duct ($h_t < \delta$). Therefore, the term inside the square-root in (9) is positive, and it has two real roots.

According to (9), a 40-m surface duct with $\Delta M = 20$ has $\theta^T_{\max,\min} = \pm 4.64$ mrad $= \pm 0.266^\circ$ where the transmitter height is $h_t = 27$ m. We also perform RO simulations based on (8) to verify our analytical trapping beamwidth formula. Fig. 4 shows the ray trajectories for the angles that are on the boundaries. As noticed, analytically calculated trapping beamwidth is consistent with the simulations. As a result, adaptive antenna techniques can be designed for ducting channel systems to maximize the trapped power with this equation, because signal transmitted out of this beamwidth region cannot be trapped by the surface ducts. In addition, for symmetrical ducting channels, where $h_t = h_r$ and refractivity profile is range independent, the calculated trapping beamwidths form an upper and lower bound for the AOA in the ducting channel.

V. Large-Scale Path-Loss Model for Surface Ducts

Ducting channel wave propagation depends on many factors: transmitter height, receiver height, duct height, duct strength, carrier frequency, polarization, and surface conditions. PE-based methods are capable of taking all of these parameters as input. Thus, we utilize PETOOL to solve PE to estimate path-loss in surface ducts for given channel parameters. We aim to develop a path-loss model as a function of the channel parameters: transmitter height, receiver height, duct height, duct strength, and carrier frequency for the first time in the literature. Our model will be independent of polarization because the effects of polarization are not noticeable in the large scale, and we use only horizontal polarization for both of the antennas. In addition, surface is assumed as smooth sea surface.

We aim to model path-loss in ducting channel for b-LoS distances where line-of-sight (LoS) transmission is impossible in the standard atmospheric conditions. For b-LoS ducting channel, the large-scale path-loss equation is given as [45]

$$PL = A + 10\gamma \log d/d_0 + X_s \tag{10}$$

where γ is the path-loss exponent, d_0 is the b-LoS range, A is the path-loss at d_0, and X_s is the shadow fading. The b-LoS range is given by the well-known maximum LoS range equation for the standard refractivity conditions as

$$d_0 = 4.12\sqrt{h_t} + 4.12\sqrt{h_r} \tag{11}$$

where h_t and h_r are the transmitter and receiver heights, respectively.

In this section, we develop a statistical large-scale path-loss model based on PE simulations performed with PETOOL. We perform the well-known regression methods to the results of PETOOL. Similar approach can be found in [46]. In addition, the distribution of shadow fading and the coefficients of the channel parameters are determined by using the multivariate linear regression method to (10). To this end, we perform PE simulations for the path-loss of the link for different channel conditions. Fig. 5(a) contains the path-loss results generated with PETOOL, the free space path-loss, and the fitted line to the PETOOL results for (10) with simulation parameters: 500-km range, 40-m surface duct, 27-m transmitter and receiver, 10-GHz carrier frequency, and 20-M-unit duct strength and horizontal polarization. For the regression line fitting for (10), we utilize the least-square fitting. Deviations from the fitting line are treated as shadow fading, and the distribution of shadow fading can be seen in Fig. 5(b). Shadowed regions can be clearly seen in Fig. 3.

Since path-loss enhancements with atmospheric ducts are most effective when both of the antennas are in ducting layer [28], we assume that both transmitter and receiver are located within surface duct. To develop the large-scale path-loss model, we perform extensive simulations by varying the channel parameters: carrier frequency ($f = 5{-}15$ GHz), duct height ($\delta = 10{-}60$ m), duct strength rate ($\Delta M/\delta = 0.1{-}0.3$ M-unit/m), transmitter height ($h_t = 0{-}\delta$ m), and receiver height ($h_r = 0{-}\delta$ m). The remaining of the section includes the derivation of the coefficients and the statistical distribution of the large-scale path-loss model parameters: A, γ, and X_s.

A. A Parameter

After performing a number of simulations using PETOOL, we tried to find the statistical distribution of each parameter. Since ducting channel that we are trying to model is symmetric, the effect of transmitter and receiver antenna heights can be modeled with the difference between them $\Delta h = h_t - h_r$. We use multivariate regression analysis in the least-square error

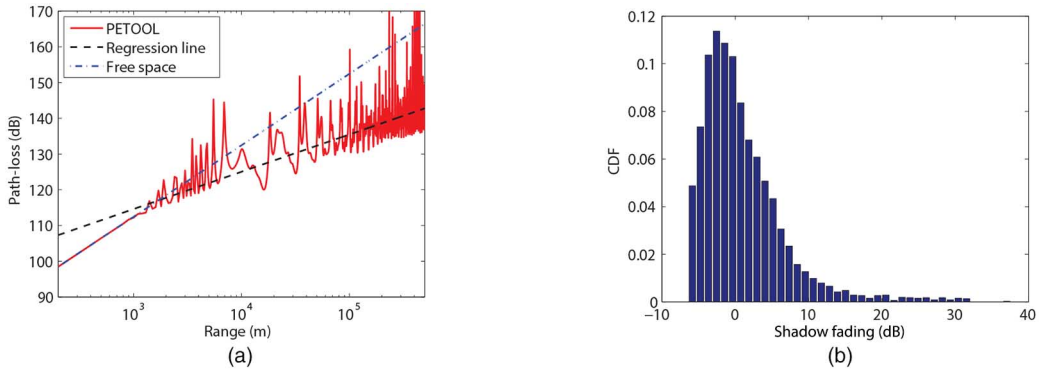

Fig. 5. Path-loss results for (a) regression method and (b) distribution of the shadow fading.

sense to find the coefficients of each channel parameter. A parameter is modeled as

$$\begin{bmatrix} 1 & \vdots & \vdots & \vdots & \vdots \\ \vdots & \Delta h_i & \delta_i & f_i & \Delta m \\ 1 & \vdots & \vdots & \vdots & \vdots \end{bmatrix} \begin{bmatrix} \alpha_A \\ \beta_A \\ \kappa_A \\ \xi_A \\ \varrho_A \end{bmatrix} = \begin{bmatrix} \vdots \\ A_i \\ \vdots \end{bmatrix} \tag{12}$$

where Δh is the height difference between the transmitter and the receiver, δ is the duct height, f is the carrier frequency, Δm is the change in the modified refractivity index per m, and A_i is the resulting value for each simulation case. By performing multivariate regression analysis in the least-square error sense, the resulting coefficients are found as $\alpha_A = 123.34$ dB, $\beta_A = 0.015$ dB/m, $\kappa_A = 0.13$ dB/m, $\xi_A = 8.66 \times 10^{-4}$ dB/MHz, and $\varrho_A = -12.83$ dB$\times$m. The variation (error) of A from the regression model is found as

$$\Delta A = \begin{bmatrix} \vdots \\ A_i \\ \vdots \end{bmatrix} - \begin{bmatrix} 1 & \vdots & \vdots & \vdots & \vdots \\ \vdots & \Delta h_i & \delta_i & f_i & \Delta n \\ 1 & \vdots & \vdots & \vdots & \vdots \end{bmatrix} \begin{bmatrix} \alpha_A \\ \beta_A \\ \kappa_A \\ \xi_A \\ \varrho_A \end{bmatrix}. \tag{13}$$

Fig. 6(a) represents the deviation of A from our model, and ΔA clearly shows a Gaussian distribution with the zero mean and standard deviation $\sigma_{\Delta A} = 2.39$ dB. Therefore, A can be represented as

$$A\,\text{dB} = \alpha_A + \beta_A \Delta h + \kappa_A \delta + \xi_A f + \varrho_A \Delta m + \sigma_{\Delta A} x \tag{14}$$

where x is zero mean unit variance Gaussian random variable.

B. γ Parameter

By the same method, γ parameter is modeled as

$$\begin{bmatrix} 1 & \vdots & \vdots & \vdots & \vdots \\ \vdots & \Delta h_i & \delta_i & f_i^2 & \Delta m \\ 1 & \vdots & \vdots & \vdots & \vdots \end{bmatrix} \begin{bmatrix} \alpha_\gamma \\ \beta_\gamma \\ \kappa_\gamma \\ \xi_\gamma \\ \varrho_\gamma \end{bmatrix} = \begin{bmatrix} \vdots \\ \gamma_i \\ \vdots \end{bmatrix}. \tag{15}$$

According to the regression results, the resulting coefficients are found as $\alpha_\gamma = 1.3$, $\beta_\gamma = 2 \times 10^{-3}$ 1/m, $\kappa_\gamma = -2.9 \times 10^{-3}$ 1/m, $\xi_\gamma = -3.47 \times 10^{-10}$ 1/MHz, $\varrho_\gamma = -0.58$ m. The coefficients β_γ and κ_γ result in too low values when they are multiplied with their parameters. Therefore, the effects of these factors can be neglected in the regression method. In (15), the frequency term is squared in order to make the error term as close as possible to the Gaussian distribution, and as can be seen in Fig. 6(b), $\Delta\gamma$ has a Gaussian distribution with zero mean and $\sigma_{\Delta\gamma} = 0.066$. In addition, the negative ϱ_γ indicates that increasing duct strength reduces the path-loss exponent. Therefore, γ can be modeled as

$$\gamma = \alpha_\gamma + \xi_\gamma f^2 + \varrho_\gamma \Delta m + \sigma_{\Delta\gamma} y \tag{16}$$

where y is the zero mean unit variance Gaussian random variable.

C. Shadowing Fading

As shown in Fig. 5(a), there is a significant shadow fading in the link, and also the distribution of the shadow fading is shown in Fig. 5(b). The best-fitted distribution for the shadow fading in the channel can be found with the Kullback–Leibler divergence (KLD) [47]. Let P and Q be the two distributions, and the divergence of Q from P can be calculated as

$$D_{KL}(P||Q) = \sum_i \ln \frac{P(i)}{Q(i)} P(i). \tag{17}$$

$D_{KL}(P||Q)$ takes lower values when the two distributions get closer, and it becomes 0 for the identical distributions.

We generate various distributions with MATLAB and use (17) to determine how close the generated distributions to the shadow fading are. The simulation results for the possible distributions can be found in Table I. According to our results, the Weibull distribution best matches with the shadow fading for surface ducts. Therefore, the shadow fading in the channel is modeled with log-Weibull distribution which is also known as Gumbel distribution.

The PDF of the Weibull distribution can be represented as

$$f(x;\lambda,k) = \begin{cases} \frac{k}{\lambda}\left(\frac{x}{\lambda}\right)^{k-1} e^{-(x/\lambda)^k}, & x \geq 0 \\ 0, & x < 0 \end{cases} \tag{18}$$

where $k > 0$ is the shape parameter and $\lambda > 0$ is the scale parameter. We perform the multivariate regression analysis to find the distribution of k and λ as well.

We use the same methodology as in A and γ parameters. Again, the parameters with slight effects are neglected and only

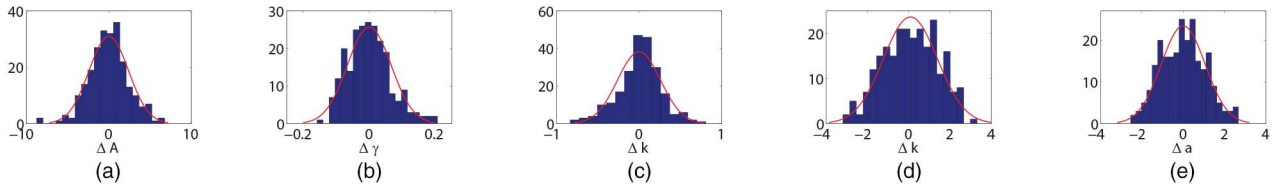

Fig. 6. Distributions for the deviations from our multivariate regression model. (a) Distribution of ΔA. (b) Distribution of $\Delta\gamma$. (c) Distribution of Δk. (d) Distribution of $\Delta\lambda$.

TABLE I
KLD RESULTS

Type of ditribution	KLD
Normal distribution	1.3436
Rayleigh distribution	0.1954
Weibull distribution	**0.0209**
Gamma distribution	0.0283
Generalized extreme value distribution	0.0887
Nakagami distribution	0.0574

the final results are presented for the remaining multivariate fitting results. With the multivariate linear regression analysis, the k parameter can be given as

$$k = \alpha_k + \xi_k f^3 + \varrho_k \Delta m + \sigma_{\Delta k} z \tag{19}$$

where z is the zero mean and unit variance Gaussian random variable. $\alpha_k = 0.1792$, $\xi_k = 3.36 \times 10^{-14}$ 1/MHz, and $\varrho_k = 1.85$ m. The deviation of k from our model can be found in Fig. 6(c), and this deviations can be modeled with Gaussian distribution with zero mean $\sigma_{\Delta k} = 0.26$.

The λ parameter can be modeled as

$$\lambda = \alpha_\lambda + \beta_\lambda \delta + \xi_\lambda f^3 + \varrho_\lambda \Delta m + \sigma_{\Delta\lambda} q \tag{20}$$

where q is the zero mean and unit variance Gaussian random variable: $\alpha_\lambda = -1.94$, $\kappa_\lambda = 0.176$ 1/m, $\xi_\lambda = 1.09 \times 10^{-12}$ 1/MHz. Fig. 6(d) shows the deviations of the λ from our model, and it has Gaussian distribution with zero mean and $\sigma_{\Delta\lambda} = 1.45$.

As noticed in Fig. 5(b), the shadow fading values can be negative. However, since the Weibull distribution takes only positive values, we first shift the shadow fading to the right by Δa and perform the distribution fitting. To this end, Δa can be represented as

$$\Delta a \,\mathrm{dB} = \alpha_a + \beta_a \delta + \kappa_a f + \varrho \Delta m + \sigma_{\Delta a} w \tag{21}$$

where w is the zero mean and unit variance Gaussian random variable. The resulting values of the $\alpha_a = 3.27$ dB, $\kappa_a = -0.14$ 1/m, $\xi_a = 3.2 \times 10^{-4}$ 1/MHz, and $\sigma_{\Delta a} = 1.07$ dB as can be seen in Fig. 6(e).

D. Large-Scale Path-Loss Model

By combining (10), (14), (16), and (21), the statistical large-scale path-loss equation is found as

$$\begin{aligned} PL &= A + 10\gamma_{\Delta h} \log d/d_0 + X_s \\ PL &= \alpha_A + \beta_A \Delta h + \kappa_A \delta + \xi_A f + \varrho_A \Delta m + \sigma_{\Delta A} x \\ &\quad + 10(\alpha_\gamma + \xi_\gamma f^2 + \varrho_\gamma \Delta m + \sigma_{\Delta\gamma} y) \log d/d_0 \\ &\quad + W + \alpha_a + \beta_a \delta + \kappa_a f + \varrho \Delta m + \sigma_{\Delta a} z \end{aligned} \tag{22}$$

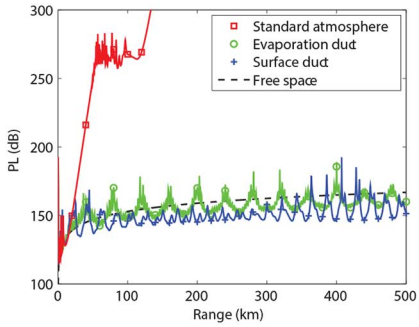

Fig. 7. Path-loss versus range for standard atmosphere, free space, and atmospheric ducts.

where x, y, and z are the zero mean unit variance independent normal random variables and W has the Weibull distribution with k in (19) and λ in (20).

VI. SIMULATION RESULTS

In this section, we present the simulation results with the PE methods and RO methods. In addition, the results of the large-scale path-loss model is compared with the PE results. We present link budget calculations for surface ducts to predict the communication ranges for given channel parameters.

A. Simulation Results With PEM

We utilize PETOOL to perform the PE simulations as described in Section IV-A. Fig. 7 presents the path-loss versus range for different atmospheric ducts, the free space and the standard atmosphere at 10.5 GHz, 5 m transmitter and receiver, and horizontal polarizations. As noticed, the curves for 40-m evaporation duct and 40-m surface duct ($\Delta M = 10$ M-unit) outperform the standard atmosphere in terms of path-loss values. In addition, surface ducts have strong shadow fading compared to the evaporation ducts.

Fig. 8(a) shows the path-loss for a 40-m surface duct (20 M-units) as a function of the carrier frequency and receiver height. As noticed, the lower frequencies 3–5 GHz have significantly higher trapping capabilities compared to the evaporation ducts [3], [16]. This is one of the main difference between surface ducts and evaporation ducts in terms of channel modeling because evaporation ducts provide lowest path-loss values near 10 GHz. Surface ducts show higher trapping capabilities over evaporation ducts due to the sharp refractivity curve of surface ducts as described in Section III.

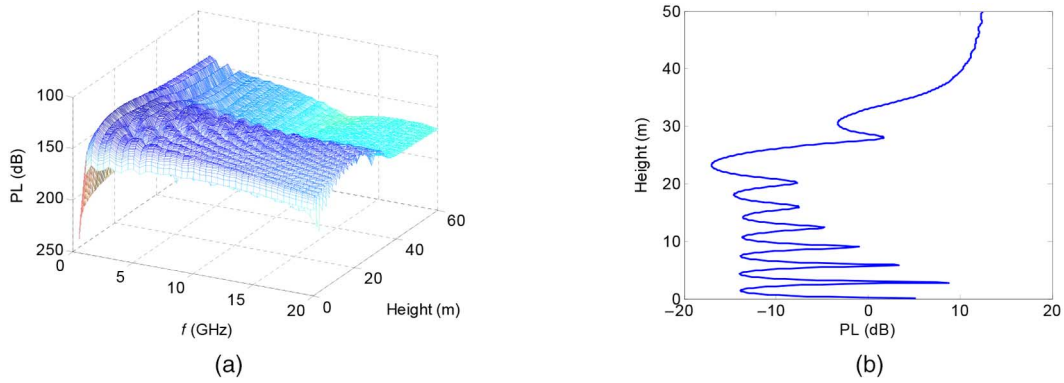

Fig. 8. Path-loss results for 40-m surface duct, 27-m transmitter height with PETOOL. (a) Path-loss versus receiver height and frequency at 100-km range. (b) Receiver height versus path-loss at 100-km range.

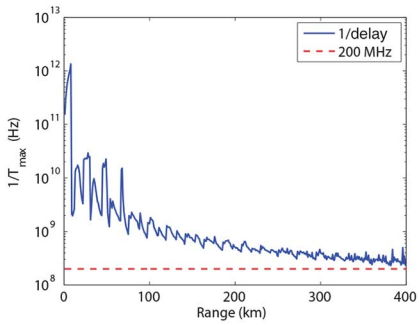

Fig. 9. $1/T_{max}$ spread for a 40-m surface duct.

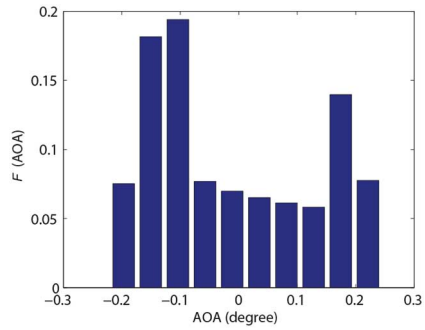

Fig. 10. Histogram of AOA for a 40-m surface duct.

Fig. 8(b) presents the path-loss values as a function of receiver height. As noticed, the path-loss values for the surface duct is significantly lower compared to the free space path-loss up to 18 dB. However, the power levels have fading with respect to the vertical height. This condition is caused by the constructive/destructive interference of the delayed signals. The delay spread of the channel should be examined in order to determine the fading behavior of the channel. Therefore, the next section presents the RO results to analyze the delay spread of the ducting channel.

B. Simulation Results With ROM

Using the calculated ray trajectories as in Fig. 3(b), delay spreads and AOAs of the received rays can be calculated. Fig. 9 presents $1/T_{max}$ in Hz versus the range for 27-m transmitter and receiver with a 40-m surface duct ($\Delta M = 20$ M-units), where T_{max} is the maximum delay spread. As noticed from the figure, $1/T_{max}$ value is higher than 200 MHz line up to 400 km. Since the channel bandwidth should be much lower than $1/T_{max}$ for a channel to have flat fading, the ducting channel can be assumed as a flat fading channel up to 400 km with 20 MHz bandwidth.

Fig. 10 presents the AOA of the ducting channel for 27-m transmitter and receiver with a 40-m surface duct ($\Delta M = 20$ M-units). As noticed, the AOA results are bounded by the analytical trapping beamwidth value of 0.266° calculated previously in Section IV-B2.

C. Large-Scale Path-Loss Model

We compare the results of our large-scale path-loss model with PETOOL for verification. The following channel parameters are utilized in the simulations: $f = 10$ GHz, $h_t = h_r = 20$, $\delta = 40$ m, $\Delta M = 20$ M-unit, horizontal polarization. Fig. 11 includes the comparison of the results in the upper figures. As noticed, our model can predict the level of the path loss for each range. The lower figures show the distribution of the deviations from our proposed model which can be modeled as the small-scale fading. As noticed, the normalized deviations can be modeled with Rayleigh distribution, and the distribution becomes closer to the Rayleigh distribution with the increasing range.

D. Link Budget Calculations

The link budget calculations are presented in this section, and the following parameters are utilized in the b-LoS channel with surface ducts:

1) transmit power (P_t) = 30 dBm (1 W);
2) antenna gains ($G_{t,r}$) = 30 dB;
3) cable losses (L_q) = 10 dB.

Received power is given by

$$P_{rdBm} = P_{tdBm} + G_{tdB} - PL_{dB} + G_{rdB} - L_{q_{dB}}. \quad (23)$$

The modern modems requires a minimum received power of -80 dBm to operate at Mbps data rates [48]. Thus, the maximum PL that can provide the communication link is found as

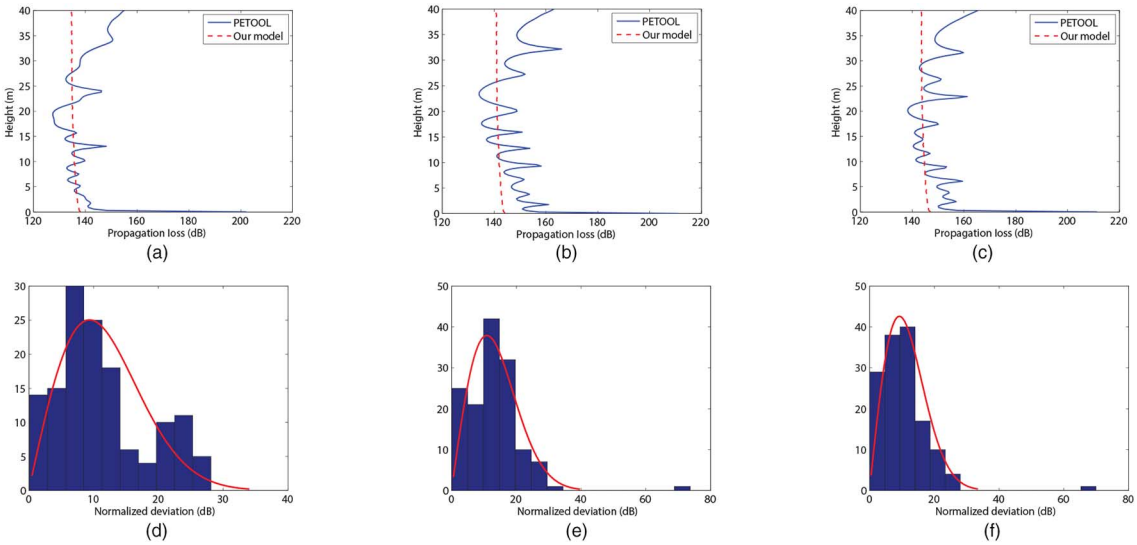

Fig. 11. Comparison of our large-scale path-loss model and PETOOL results. Comparision at (a) 50; (b) 250; and (c) 500 km. Histogram of deviation at (d) 50; (e) 250; and (f) 500 km.

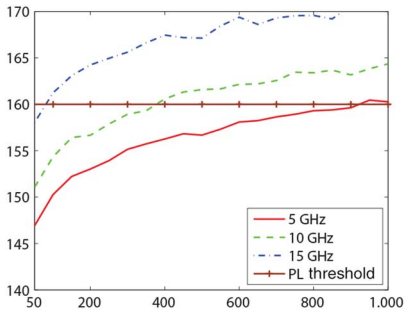

Fig. 12. Link budget analysis for surface ducts.

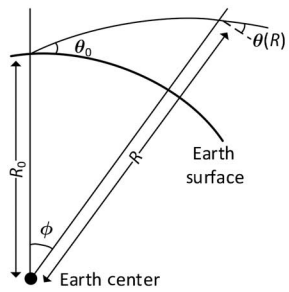

Fig. 13. Ray trajectory for refractive path.

160 dB (PL threshold) by (23). Fig. 12 presents the path-loss curves for different frequencies for 90% not exceeded of the time and PL threshold for a 40-m surface duct ($\Delta M = 10$), 27-m transmitter and receiver. As noticed, 10 GHz can provide communication links up to 1000 km. Lower frequencies can provide higher ranges. For high duct heights (>20 m), lower frequencies have better trapping capabilities as also experimentally presented in [49]. Since duct height of surface ducts are generally between 20 and 60 m as in [11], [12], lower frequencies will show better trapping capabilities for the surface ducts. However, duct height for evaporation ducts is mostly smaller than 20 m. Thus, trapping capability of evaporation ducts significantly differs from the surface ducts as presented in [2] and [16].

VII. Conclusion and Future Work

In this work, we develop a large-scale path-loss model for the surface ducts and analyze the delay spreads and AOA of the ducting channel. According to our results, the ducting channel can be used as communication medium up to 1000 km, and the small-scale fading in the channel shows Rayleigh fading. In addition, our RO methods can be utilized to estimate the fading behavior of the channel. Upper and lower bounds for the AOA of the channel can be estimated with the effective trapping beamwidth equation.

Appendix A
Derivation of the Eikonal Equation

To derive (6), the earth radius transformation is utilized as shown in Fig. 13 [39]. Therefore, the well-known Snell's equation for the stratified atmosphere is given as

$$R_0 n(z)\cos(\theta) = (R_0 + \Delta R)n(z + \Delta z)\cos(\theta - \Delta\theta). \quad (24)$$

Since the index of refraction is modeled with a bilinear curve for the surface ducts, (24) is represented as

$$R_0 n(z)\cos(\theta) = (R_0 + \Delta R)(n(z) - \frac{dn}{dz}\Delta z)\cos(\theta - \Delta\theta). \quad (25)$$

We know that Δz and $\Delta\theta$ will be small because the step sizes in the simulations will be low. Therefore, their squares and multiplications will give zero $\Delta z^2 = \Delta\theta^2 = \Delta z\Delta\theta = 0$. For small $\Delta\theta$, $\cos(\Delta\theta) = 1$ and $\sin(\Delta\theta) = \Delta\theta$. By knowing these conditions, (25) is simplified as

$$R_0 n(z)\cos(\theta) = R_0 n(z)\cos(\theta) - R_0\frac{dn}{dz}\Delta z\cos(\theta) + \Delta z n(z)\cos(\theta) + R_0 n(z)\Delta\theta\sin(\theta) \quad (26)$$

$$\frac{1}{n(z)}\frac{dn}{dz} = \frac{1}{R_0} + \frac{\Delta\theta}{\Delta z}\tan(\theta) \quad (27)$$

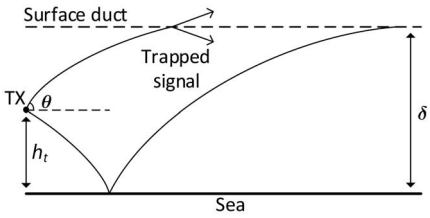

Fig. 14. Trajectory of a trapped ray.

where $\frac{\Delta\theta}{\Delta z}\tan(\theta) = \frac{\Delta\theta}{\Delta z}\frac{\Delta z}{\Delta x} = \frac{\Delta\theta}{\Delta x}$ [43]. As Δx goes to 0, $\frac{\Delta\theta}{\Delta x} = \frac{d\theta}{dx}$. Since $\theta = \frac{dz}{dx}$, the Eikonal equation for the Earth radius transformation can be represented as

$$\frac{1}{n(z)}\frac{dn}{dz} - \frac{1}{R_0} = \frac{d^2z}{dx^2}. \tag{28}$$

Appendix B
Derivation of Ray Trajectory Equation

The ray trajectory (7) can be solved as

$$\frac{d^2z}{dx^2} = \frac{1}{n(0)}\frac{dn}{dz} - \frac{1}{R_0} \tag{29}$$

$$z'' = \frac{1}{n(0)}\frac{dn}{dz} - \frac{1}{R_0} \tag{30}$$

$$z' = \left(\frac{1}{n(0)}\frac{dn}{dz} - \frac{1}{R_0}\right)x + \theta \tag{31}$$

$$z = \frac{1}{2}\left(\frac{1}{n(0)}\frac{dn}{dz} - \frac{1}{R_0}\right)x^2 + \theta x + h_t. \tag{32}$$

Appendix C
Derivation of Trapping Beamwidth Derivations

In the trapping beamwidth calculations, it is assumed that antennas has 0 elevation angle. The procedure is designed to find the maximum beamwidth that can be trapped by the surface ducts with respect to duct height (δ) and transmitter antenna height (h_t) as shown in Fig. 14.

Starting form (8), let us denote $K = \frac{1}{2}\left(\frac{1}{n(0)}\frac{dn}{dz} - \frac{1}{R_0}\right)$ and we can write the following equations:

$$z = Kx^2 + \theta x + h_t \tag{33}$$

$$z + \Delta z = K(x + \Delta x)^2 + \theta(x + \Delta x) + h_t. \tag{34}$$

If we subtract the above equations, the result is given as

$$\Delta z = \Delta x^2 K + 2x\Delta x K + \theta\Delta x \tag{35}$$

$$\frac{\Delta z}{\Delta x} = \Delta x K + 2xK + \theta. \tag{36}$$

At the boundary layer, the trapped ray will have zero Δz for very small step sizes because the trapped signal will first become parallel with the surface and then propagate downward. In addition, for small step sizes, $K\Delta x$ term will be nearly zero. Therefore, (36) is simplified as

$$-2xK = \theta^T \tag{37}$$

$$x = -(\theta^T/2K). \tag{38}$$

Therefore, at the duct height (boundary $z = \delta$), (33) is represented as

$$z = \delta = Kx^2 + \theta^T x + h_t. \tag{39}$$

By combining (38) and (39), the maximum and minimum effective trapping beamwidths are found as

$$\delta = (1/4K){\theta^T}^2 - (1/2K){\theta^T}^2 + h_t \tag{40}$$

$$\delta - h_t = -(1/4K){\theta^T}^2 \tag{41}$$

$${\theta^T}^2 = 4K(h_t - \delta) \tag{42}$$

$$\theta^T_{max,min} = \pm\sqrt{4K(h_t - \delta)} \tag{43}$$

$$\theta^T_{max,min} = \pm\sqrt{2\left(\frac{1}{n(0)}\frac{dn}{dz} - \frac{1}{R_0}\right)(h_t - \delta)}. \tag{44}$$

Since the transmitter located within duct both $\frac{dn}{dz}$ and $h_t - \delta$ terms are negative, so this equation will have two real roots.

References

[1] H. V. Hitney, J. H. Richter, R. A. Pappert, K. D. Anderson, and G. B. Baumgartner Jr., "Tropospheric radio propagation assessment," *Proc. IEEE*, vol. 73, no. 2, pp. 265–283, Feb. 1985.

[2] G. S. Woods, A. Ruxton, C. Huddlestone-Holmes, and G. Gigan, "High-capacity, long-range, over ocean microwave link using the evaporation duct," *IEEE J. Ocean. Eng.*, vol. 34, no. 3, pp. 323–330, Jul. 2009.

[3] E. Dinc and O. B. Akan, "Beyond-line-of-sight communications with ducting layer," *IEEE Commun. Mag.*, vol. 52, no. 10, pp. 37–43, Oct. 2014.

[4] I. Sirkova, "Brief review on PE method application to propagation channel modeling in sea environment," *Cent. Eur. J. Eng.*, vol. 2, no. 1, pp. 19–38, 2012.

[5] J. H. Richter, "Sensing of radio refractivity and aerosol extinction," in *Proc. Int. Geosci. Remote Sens. Symp.*, vol. 1, Pasadena, CA, USA, Aug. 8–12, 1994, pp. 381–385.

[6] A. Willitsford and C. R. Philbrick, "Lidar description of the evaporative duct in ocean environments," *Proc. SPIE*, vol. 5885, Bellingham, WA, USA, Sep. 2005.

[7] R. M. Hodur, "The naval research laboratorys coupled ocean/atmosphere mesoscale prediction system (COAMPS)," *Mon. Weather Rev.*, vol. 125, no. 7, pp. 1414–1430, 1996.

[8] A. R. Lowry, C. Rocken, S. V. Sokolovskiy, and K. D. Anderson, "Vertical profiling of atmospheric refractivity from ground-based GPS," *Radio Sci.*, vol. 37, no. 3, pp. 1041–1059, 2002.

[9] L. T. Rogers, C. P. Hattan, and J. K. Stapleton, "Estimating evaporation duct heights from radar sea echo," *Radio Sci.*, vol. 35, no. 4, pp. 955–966, 2000.

[10] P. Gerstoft, L. T. Rogers, J. L. Krolik, and W. S. Hodgkiss, "Inversion for refractivity parameters from radar sea clutter," *Radio Sci.*, vol. 38, no. 3, pp. 1–22, Apr. 2003.

[11] S. S. Mentes and Z. Kaymaz, "Investigation of surface duct conditions over Istanbul, Turkey," *J. Appl. Meteorol. Climatol.*, vol. 46, pp. 318–338, 2007.

[12] S. M. Babin "Surface duct height distributions for Wallops Island, Virginia, 1985–1994," *J. Appl. Meteorol.*, vol. 35, pp. 86–93, 1996.

[13] L. M. Brekhovskikh, *Waves in Layered Media*, 2nd ed. New York, NY, USA: Academic Press, 1980.

[14] G. B. Baumgartner, H. V. Hitney, and R. A. Pappert, "Duct propagation modeling for the integrated refractive effects prediction system (IREPS)," *IEE Proc. F Commun. Radar Signal Process.*, vol. 130, no. 7, pp. 630–642, Dec. 1983.

[15] R. H. Hardin and F. D. Tappert, "Application of the split-step Fourier method to the numerical solution of nonlinear and variable coefficient wave equations," *SIAM Rev.*, vol. 15, p. 423, 1973.

[16] A. Iqbal and V. Jeoti, "Feasibility study of radio links using evaporation duct over sea off Malaysian shores," in *Proc. Int. Conf. Intell. Adv. Syst. (ICIAS)*, Jun. 2010, pp. 1–5.

[17] S. D. Gunashekar, E. M. Warrington, and D. R. Siddle, "Long-term statistics related to evaporation duct propagation of 2 GHz radio waves in the English Channel," *Radio Sci.*, vol. 45, 2010.
[18] Wayne L. Patterson, *Users Manual for Advanced Refractive Effects Prediction System (AREPS)*. San Diego, CA, USA: Space Naval Warfare Syst. Center, 2004, pp. 1–7.
[19] A. E. Barrios, "Considerations in the development of the advanced propagation model (APM) for U.S. Navy applications," in *Proc. Int. Radar Conf.*, 2003, pp. 77–82.
[20] A. E. Barrios, "Advanced propagation model," in *Proc. Battlespace Atmos. Conf.*, Dec. 1997, pp. 483–490.
[21] A. E. Barrios, W. L. Patterson, and R. A. Sprague, "Advanced propagation model (APM) version 2.1.04," Computer Software Configuration Item (CSCI) Documents SSC San Diego, Tech. Doc. 3214, 2007.
[22] A. E. Barrios, K. Anderson, and G. Lindem, "Low altitude propagation effects–A validation study of the advanced propagation model (APM) for mobile radio applications," *IEEE Trans. Antennas Propag.*, vol. 54, no. 10, pp. 2869–2877, Oct. 2006.
[23] O. Ozgun, G. Apaydin, M. Kuzuoglu, and L. Sevgi, "PETOOL: MATLAB-based one-way and two-way split-step parabolic equation tool for radiowave propagation over variable terrain," *Comput. Phys. Commun.*, vol. 182, no. 12, pp. 2638–2654, Dec. 2011.
[24] K. D. Anderson, "Evaporation duct communication: Test plan," Naval Ocean Systems Center, San Diego, CA, USA, Tech. Doc. 2033, 1991.
[25] K. D. Anderson and L. T. Rogers, "Evaporation duct communication: Test plan II," Naval Ocean Systems Center, San Diego, CA, USA, Tech. Doc. 1460, 1991.
[26] L. T. Rogers and K. D. Anderson, "Evaporation duct communication: Measurement results," Naval Ocean Systems Center, San Diego, CA, USA, Tech. Doc. 1571, 1993.
[27] K. D. Anderson, "Radar detection of low-altitude targets in a maritime environment," *IEEE Trans. Antennas Propag.*, vol. 43, no. 6, pp. 609–613, Jun. 1995.
[28] G. D. Dockery, "Modeling electromagnetic wave propagation in the troposphere using the parabolic equation," *IEEE Trans. Antennas Propag.*, vol. 36, no. 10, pp. 1464–1470, Oct. 1988.
[29] B. R. Bean and E. J. Dutton, *Radio Meteorology*. New York, NY, USA: Dover, 1966.
[30] R. A. Paulus, "Evaporation duct effects on sea clutter," *IEEE Trans. Antennas Propag.*, vol. 38, no. 11, pp. 1765–1771, Nov. 1990.
[31] "ITU-R's Rec. P. 453-10: The radio refractive index: Its formula and refractivity data," ITU-R, 2012.
[32] V. A. Fock, "Solution of the problem of propagation of electromagnetic waves along the earths surface by method of parabolic equations," *J. Phys. USSR*, vol. 10, pp. 13–35, 1946.
[33] M. Levy, *Parabolic Equation Methods for Electromagnetic Wave Propagation*. London, U.K.: Inst. Elect. Eng., 2000.
[34] G. D. Dockery and J. R. Kuttler, "An improved-boundary algorithm for Fourier split-step solutions of the parabolic wave equation," *IEEE Trans. Antennas Propag.*, vol. 44, no. 12, pp. 1592–1599, Dec. 1996.
[35] J. R. Kuttler and G. D. Dockery, "Theoretical description of the parabolic approximation Fourier split-step method of representing electromagnetic propagation in the troposphere," *Radio Sci.*, vol. 26, pp. 381–393, 1991.
[36] A. E. Barrios, "Parabolic equation modeling in horizontally inhomogeneous environments," *IEEE Trans. Antennas Propag.*, vol. 40, no. 7, pp. 791–797, Jul. 1992.
[37] R. K. Crane, *Propagation Handbook for Wireles*. Boca Raton, FL, USA: CRC Press, 2003.
[38] R. Akbarpour and A. R. Webster, "Ray-tracing and parabolic equation methods in the modeling of a tropospheric microwave link," *IEEE Trans. Antennas Propag.*, vol. 53, no. 11, pp. 3785–3791, Nov. 2005.
[39] S. A. Parl, "Characterization of multipath parameters for line-of-sight microwave propagation," *IEEE Trans. Antennas Propag.*, vol. 31, no. 6, pp. 938–948, Nov. 1983.
[40] L. Pickering and J. K. DeRosa, "Refractive multipath model for line-of-sight microwave relay links," *IEEE Trans. Commun.*, vol. 27, no. 8, pp. 1174–1182, Aug. 1979.
[41] A. R. Webster, "Raypath parameters in tropospheric multipath propagation," *IEEE Trans. Antennas Propag.*, vol. 30, no. 4, pp. 796–800, Jul. 1982.
[42] A. R. Webster, "Angles-of-arrival and delay times on terrestrial line-of-sight microwave links," *IEEE Trans. Antennas Propag.*, vol. 31, no. 1, pp. 12–17, Jan. 1983.
[43] J. A. Caicedo, "Propagation in evaporation ducts with applications to detecting sea-surface targets using MIMO radar systems," Univ. Florida, FL, Fall 2011.
[44] C. Yardim, "Statistical estimation and tracking of refractivity from radar clutter," Ph.D. dissertation, Univ. California, San Diego, CA, Mar. 2007.
[45] A. Goldsmith, *Wireless Communications*. Cambridge, U.K.: Cambridge Univ. Press, 2005.
[46] V. Erceg *et al.*, "An empirically based path loss model for wireless channels in suburban environments," *IEEE J. Sel. Areas Commun.*, vol. 17, no. 7, pp. 1205–1211, Jul. 1999.
[47] S. Boyd and L. Vandenberghe, *Convex Optimization*. Cambridge, U.K.: Cambridge Univ. Press, 2004.
[48] General Dynamics, "Troposcatter modem," Model TM-20 datasheet, Oct. 2008.
[49] H. V. Hitney and R. Vieth, "Statistical assessment of evaporation duct propagation," *IEEE Trans. Antennas Propag.*, vol. 38, no. 6, pp. 794–799, Jun. 1990.

Ergin Dinc (S'12) received the B.Sc. degree in electrical and electronics engineering from Bogazici University, Istanbul, Turkey, in 2012. He is currently pursuing the Ph.D. degree at the Electrical and Electronics Engineering Department, Koc University, Istanbul, Turkey.

He is currently a Research Assistant with the Next-Generation and Wireless Communications Laboratory (NWCL), Istanbul, Turkey. His research interests include communication theory, beyond-line-of-sight (b-LoS) communications with troposcatter, and atmospheric ducts.

Ozgur B. Akan (M'00–SM'07) received the Ph.D. degree in electrical and computer engineering from the Broadband and Wireless Networking Laboratory, School of Electrical and Computer Engineering, Georgia Institute of Technology, Atlanta, GA, USA, in 2004.

He is currently a Full Professor with the Department of Electrical and Electronics Engineering, Koc University, Istanbul, Turkey, and the Director of the Next-Generation and Wireless Communications Laboratory, Istanbul, Turkey. His research interests include wireless communications, nano-scale and molecular communications, and information theory.

He is an Associate Editor of the IEEE TRANSACTIONS ON COMMUNICATIONS, THE IEEE TRANSACTIONS ON VEHICULAR TECHNOLOGY, the *International Journal of Communication Systems* (Wiley), the *Nano Communication Networks Journal* (Elsevier), and the *European Transactions on Technology*.